Brain Structure and Function (2021) 226:1961–1972
https://doi.org/10.1007/s00429-021-02303-x

ORIGINAL ARTICLE

Mapping fetal brain development based on automated segmentation and 4D brain atlasing

Haotian Li[1] · Guohui Yan[2] · Wanrong Luo[1] · Tingting Liu[1] · Yan Wang[1] · Ruibin Liu[1] · Weihao Zheng[1] · Yi Zhang[1,3] · Kui Li[2] · Li Zhao[4] · Catherine Limperopoulos[4] · Yu Zou[2] · Dan Wu[1]

Received: 14 January 2021 / Accepted: 19 May 2021 / Published online: 29 May 2021

Abstract

Fetal brain MRI has become an important tool for in utero assessment of brain development and disorders. However, quantitative analysis of fetal brain MRI remains difficult, partially due to the limited tools for automated preprocessing and the lack of normative brain templates. In this paper, we proposed an automated pipeline for fetal brain extraction, super-resolution reconstruction, and fetal brain atlasing to quantitatively map in utero fetal brain development during mid-to-late gestation in a Chinese population. First, we designed a U-net convolutional neural network for automated fetal brain extraction, which achieved an average accuracy of 97%. We then generated a developing fetal brain atlas, using an iterative linear and nonlinear registration approach. Based on the 4D spatiotemporal atlas, we quantified the morphological development of the fetal brain between 23 and 36 weeks of gestation. The proposed pipeline enabled the fully automated volumetric reconstruction for clinically available fetal brain MRI data, and the 4D fetal brain atlas provided normative templates for the quantitative characterization of fetal brain development, especially in the Chinese population.

Keywords U-net convolutional network · Fetal brain extraction · Chinese fetal brain atlas · Morphological development · Super-resolution reconstruction

Introduction

Magnetic resonance imaging (MRI) provides superior and versatile contrasts of the gray and white matter structures relative to other imaging modalities, such as ultrasound. It is also one of the few clinical options to examine the fetal brains with hardly known safety concerns (Chartier et al. 2019) compared to other ionizing radiation imaging methods, and its role in fetal brain examination has been recognized over the years (Griffiths et al. 2017; Weisstanner et al. 2015; Jarvis and Griffiths 2019). In utero MRI offers exquisite anatomical details of the fetal brain within millimeter resolution and has become an important tool for prenatal diagnosis, complementary to ultrasound examination (Nielsen and Scott 2017). For instance, in utero MRI plays an important role in identifying gyral and sulcal abnormalities (Rolo et al. 2011), corpus callosum dysgenesis (Glenn 2006), and abnormal cortical maturation (Fogliarini et al. 2005) in the fetal brain. Moreover, quantitative analysis of in utero images has further improved our understanding of fetal brain development (Makropoulos et al. 2018; Scott et al. 2011).

Three-dimensional (3D) high-resolution images are often required for quantitative analysis of the brain, which, however, remains challenging for in utero MRI, due to the excessive and unpredictable fetal and maternal abdominal motion. Although direct 3D imaging of the fetal brain was possible in animal studies with anesthesia, respiratory gating, navigator-based motion correction (Wu et al. 2015), and retrospective motion correction (Kochunov et al.

✉ Dan Wu
danwu.bme@zju.edu.cn

1 Key Laboratory for Biomedical Engineering of Ministry of Education, Department of Biomedical Engineering, College of Biomedical Engineering & Instrument Science, Zhejiang University, Hangzhou, Zhejiang, China

2 Department of Radiology, School of Medicine, Women's Hospital, Zhejiang University, Hangzhou, Zhejiang, China

3 Department of Neurology, The First Affiliated Hospital, Zhejiang University, Hangzhou, China

4 Center for the Developing Brain, Diagnostic Imaging and Radiology, Children's National Medical Center, Washington, DC, USA

2010), it remains extremely challenging for human studies, and clinical fetal brain MRI is predominantly performed with 2D multi-slice protocols. Slice-to-volume registration (SVR) (Rousseau et al. 2006; Jiang et al. 2007; Kainz et al. 2015) of 2D multi-slice images with the super-resolution (SR) technique (Gholipour et al. 2010; Kuklisova-Murgasova et al. 2012; Rousseau et al. 2010) is commonly used to achieve the 3D volumetric reconstruction of the fetal brains. To achieve accurate SR reconstruction, extraction of the fetal brain from in utero images is required, which relies on the manual delineation of the brain contours on 2D slices in all three orientations. This labor-intensive process inhibits large data analysis. Several brain extraction methods have been proposed and are widely available in published toolboxes, such as the Brain Extraction Tool (BET) (Jenkinson et al. 2005) and others (Cox 1996; Lin et al. 2003; Iglesias et al. 2011), which were developed for the adult brain and usually fail for the fetal brain, due to the complex in utero and abdominal tissues surrounding the fetal brain. Deep learning-based segmentation methods have been proposed in recent years (Kleesiek et al. 2016; Salehi et al. 2017; Ebner et al. 2020), which have also been extended to segment the fetal brain and achieved higher segmentation accuracy compared to the traditional approaches. Therefore, we proposed a model-based U-net (Ronneberger et al. 2015) to directly segment the fetal brain from routine clinical in utero MRI data acquired in three orientations, as a preprocessing step before 3D volumetric reconstruction.

Another challenge for in utero fetal brain MRI is that the rapid developmental changes of the fetal brain impose difficulties for radiological examinations that mainly rely on visual inspection and empirical assessment. It is essential to have normative fetal brain templates at matching gestational ages (GA) to compare with. Brain templates or atlases play an important role in quantitative image analysis. Currently, the development of fetal brain atlases is limited compared with that of neonatal, pediatric, and adult brain atlases, due to the difficulties in the acquisition and preprocessing. Initial attempts have been made. Habas et al. developed a probabilistic fetal brain MRI atlas using clinical MR scans of 20 young fetuses with GA ranging from 20.6 to 24.7 weeks (Habas et al. 2010). Serag et al. constructed a 4D atlas of the developing fetal brains between 23 and 37 weeks of gestational, using T2 weighted MR images from 80 fetuses (Serag et al. 2012a, b) (https://brain-development.org/brain-atlases/fetal-brain-atlases/fetal-brain-atlas-serag/). Gholipour et al. established an unbiased four-dimensional atlas of the fetal brain using high-resolution MRI of 81 normal fetuses between 19 and 39 weeks of gestation (Gholipour et al. 2017) and made it a public resource (http://crl.med.harvard.edu/research/fetal_brain_atlas/).

However, all the aforementioned fetal brain atlases were established in Caucasian or mixed populations. It is known that there are considerable anatomical and functional differences between Caucasian and Chinese cohorts in the pediatric, adolescent, and adult brains (Lee et al. 2005; Tang et al. 2010; Uchiyama et al. 2013). These differences likely start in the fetal period due to both genetic and environmental factors (Rao et al. 2017; Chee et al. 2009; Tang et al. 2010). Therefore, the existing atlases may not be ideal for the analysis of fetal brains in a non-Caucasian population. Given the rapid development of the fetal brain, a small difference between the subject and atlas may have a noticeable impact. Here, we generated the first version of Chinese fetal brain atlas between 23–36 weeks of gestation, which allowed us to quantitatively characterize the 3D morphological evolution of the fetal brain.

Methods

Dataset

In our study, all the data were collected retrospectively at Women's Hospital of Zhejiang University School of Medicine between the years of 2013–2019. The research protocols were approved by the local Institutional Review Board with a waiver of consent. In utero MRI images from pregnant women between 21 and 40 weeks of pregnancy were included in this study. The gestational age was dated according to the first day of the last menstrual period.

The scans were performed at a 1.5 T GE scanner (Signa Hdxt) with an 8-channel cardiac coil. No sedation or contrast agents were administered in this study. Images were acquired using the single shot Fast Spin Echo (ssFSE) or the T2-prepared balanced Steady State Free Precession (bSSFP) sequence. The ssFSE data were acquired with repetition time (TR) = 2400 ms, echo time (TE) = 130 ms, field-of-view (FOV) = 360 × 360 mm, imaging matrix = 512 × 512 (in-place resolution = 0.7 × 0.7 mm), and approximately 20 slices with slice thickness of 4 ± 0.1 mm and no slice gap. The bSSFP data were acquired at TR = 4.7 ms, TE = 2.1 ms, flip angle = 55º, FOV = 380 × 380 mm, imaging matrix = 512 × 512 (in-place resolution = 0.74 × 0.74 mm), and approximately 16 slices with slice thickness of 5 ± 0.1 mm and no slice gap.

In total, we obtained 636 stacks from 212 fetal brains (each fetus has three stacks of slices in axial, coronal, and sagittal orientations) after visual inspection for image quality. The number of stacks at each GA for axial, coronal, and sagittal scans with either bSSFP or ssFSE sequences is presented in Fig. 1. These data were used for two purposes. (1) To train the U-net based fetal brain extraction, all 636 scans were used. Note that for this purpose, the three stacks

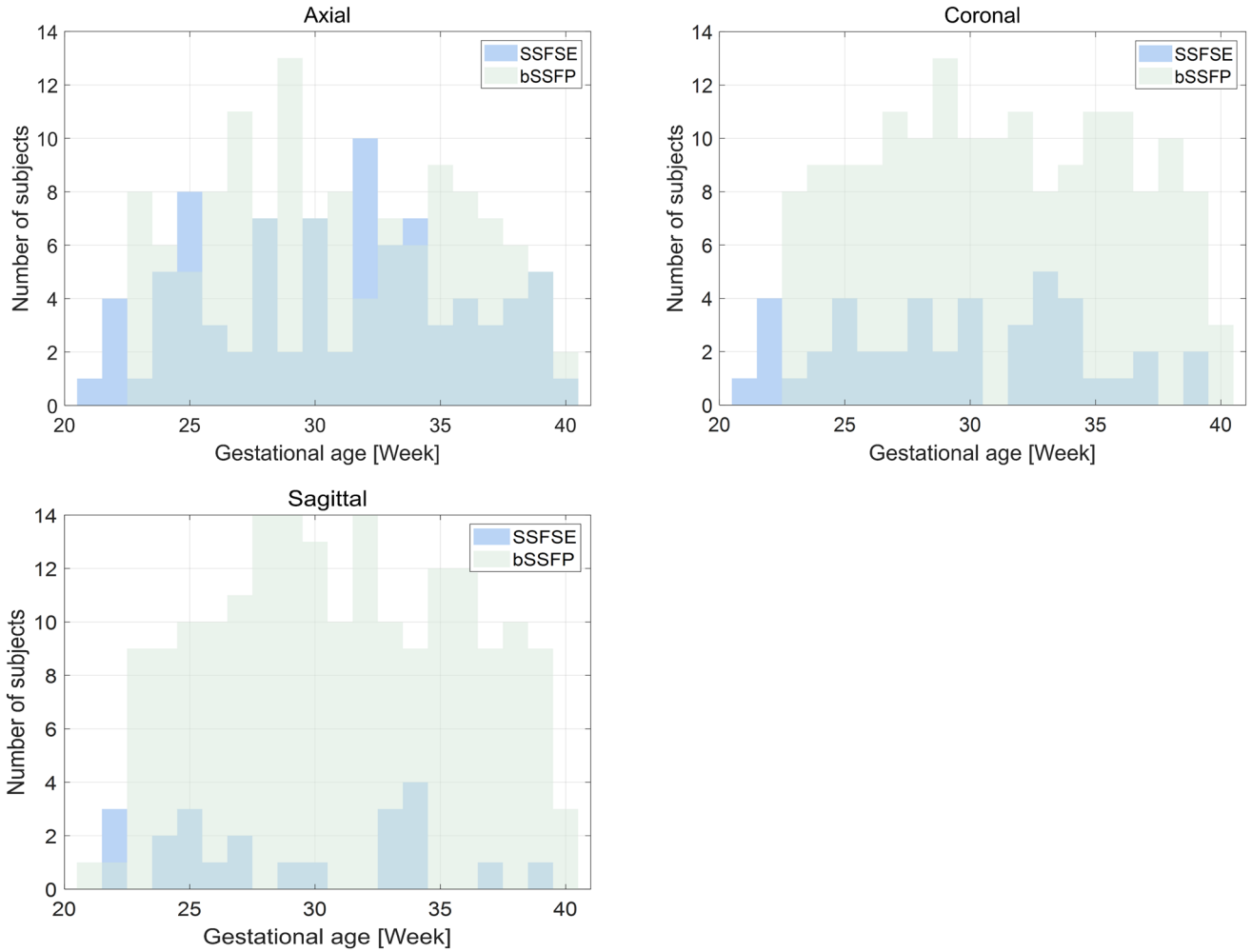

Fig. 1 Distribution of the fetal brain MRI data used for the U-net based fetal brain extraction. The images were acquired in the axial (**a**), coronal (**b**), and sagittal (**c**) orientations between 21–40 gestational weeks, by SSFSE and bSSFP sequences

of a fetal brain did not have to be of the same sequence type. Since the SSFSE and bSSFP images in this study had comparable contrasts, they were jointly used to train the U-net. (2) To build the fetal brain atlas, data acquired with bSSFP in all three orientations ($n = 95$) were used. We included only the normal-developing fetuses, and excluded fetuses with suspected fetal growth restriction based on ultrasound screening, fetal intracranial abnormalities such as ventriculomegaly, cerebral hemorrhage, chromosome abnormalities, gestational diabetes mellitus, and maternal intrauterine infections including cytomegalovirus and toxoplasmosis, and abnormalities in the rest of the body. 47 of the 95 fetal brains were diagnosed as radiologically and clinically normal by experienced radiologists and clinicians (ZY, YG, and LK). After removing 12 of the 47 fetal brains that did not have sufficient image quality after volumetric reconstruction for atlas generation (small motion artifacts or insufficient SNR), 35 normally developing fetal brains between 23 and 36 weeks of gestation were selected (five brains every two gestational weeks).

Fetal brain extraction

D U-Net architecture

The fetal brain masks were manually delineated by a trained research assistant on all 636 scans and used as the ground truth for training in the following network. Manual brain extraction took about thirty to forty minutes per fetal brain (including three orientations), depending on the GA of the fetal brain and the quality of the images.

Figure 2 shows the U-Net CNN structure for fetal brain segmentation. The U-net has an approximately symmetric structure, which consists of a contracting path and an expanding path. Each convolutional layer is followed by a ReLU nonlinear layer. In the contracting path, a 2×2

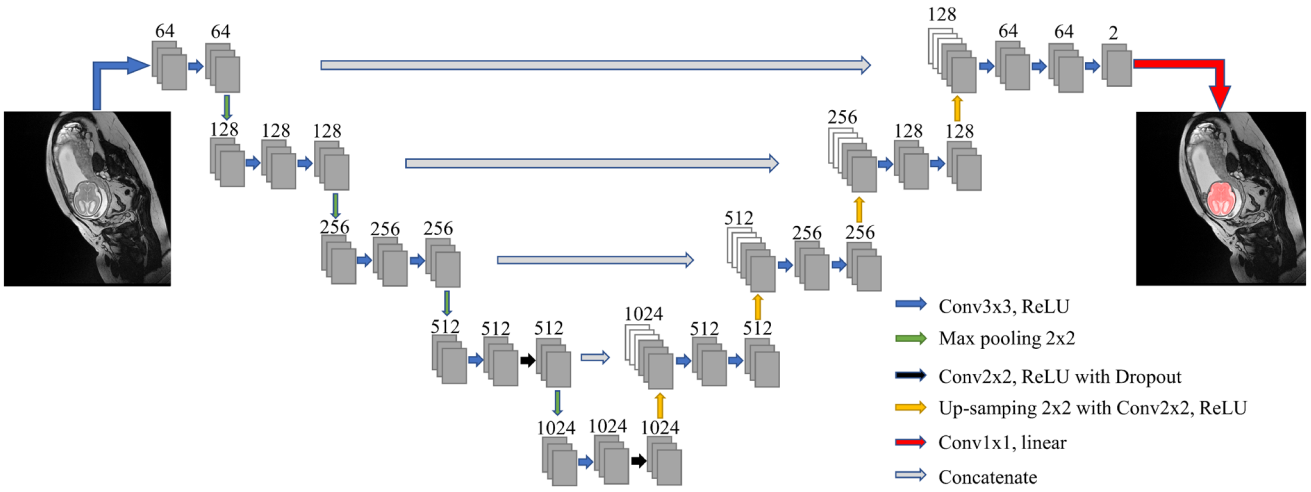

Fig. 2 The U-net convolutional network for fetal brain segmentation. The network consisted of a contraction path and an expansion path. The convolution layer was set to have a kernel size of 3×3 and stride of 2 with zero-padding. The number of features is labeled above the network layers, and the types of connection between layers are indicated in the lower right corner

max-pooling layer is applied after two 3×3 convolutional layers and the number of feature channels gets doubled. Correspondingly, the expanding path utilizes a 2×2 up-sampling layer after a convolutional operation to halve the feature channels. A dropout rate of 0.5 is used before the last pooling layer and the first up-sampling layer. The sizes of the symmetric structures between the contracting and the expanding paths are kept the same. Therefore, the outputs of the contracting path are directly concatenated with the corresponding layers of the expanding path. In the final layer, a 3×3 convolutional layer converts the feature maps to label probability, and a 1×1 convolution layer with linear output predicts the fetal brain contour.

Images acquired in three orientations were separately trained using independent U-net, which shared the same network structure. There were 212 scans from 212 fetal brains for each network, and we used individual slices as input data to the U-nets. The data were randomly divided into 6:2:2 for training, validation, and testing within each gestational week bin. Four-fold cross-validation was applied to the training and validation sets and then averaging the results from the cross-validation gave the final validation outcome. Image data in the training and validation sets were enhanced by ten times with image translation ranged 0–20 pixels, rotation ranged 0–20 degrees, random cropping, and vertical mirror symmetry (Wang and Perez 2017).

We applied the Softmax method to measure the loss function for every pixel, and the cross-entropy loss function between predicted results and ground truth was minimized on 30 epochs. The U-net network was trained using an ADAM optimizer with an initial learning rate of 1×10^{-6} that was multiplied by 0.1 for every 10 epochs. The training time was approximately six hours with four parallel Nvidia Geforce GTX2080Ti GPUs. For testing, we obtained a probability image as the output of the network, and the final mask was determined using a threshold of 0.9. The choice of threshold (between 0.1 and 0.9) did not affect the segmentation accuracy.

Evaluation of the segmentation accuracy

The test set of fetal brain images was also segmented using an open-source toolkit "NiftyMIC" (Ebner et al. 2018a, b, 2020) (https://github.com/gift-surg/NiftyMIC), which incorporates fetal brain extraction using CNNs for localization and segmentation. The neighborhood filling was performed for both the U-net and the NiftyMIC outputs to remove the holes and islands. The performance of U-Net and NiftyMIC was assessed by comparison with the manual brain segmentation based on the Dice score, intersection over union (IOU), sensitivity, and specificity in three orientations. Based on the predicted brain mask A and the ground truth mask B, the true positive (TP), false positive (FP), true negative (TN), and false negative (FN) rates were calculated, and Dice is defined as $\frac{2|A|\cap|B|}{|A|+|B|}=\frac{2TP}{2TP+FP+FN}$, IOU as $\frac{|A|\cap|B|}{|A|\cup|B|}$, specificity as $\frac{TN}{TN+FP}$, and sensitivity as $\frac{TP}{TP+FN}$.

D volumetric reconstruction

3D fetal brain images were reconstructed using an SR pipeline (Rousseau et al. 2006) based on the 2D fetal brain images extracted in three orientations. We used an open-source toolkit "BTK" (Rousseau et al. 2013) (https://github.com/rousseau/fbrain) to perform global histogram matching among the axial, sagittal, and coronal

images, non-local denoising, SVR registration, and SR reconstruction. The 3D fetal brain images were reconstructed into 0.8 mm isotropic resolution.

Generation of the fetal brain atlas

Before the atlas generation, the image intensities of individual fetal brains were normalized into 0–1 to avoid the atlas dependency on a single subject. We designed an iterative linear and nonlinear registration framework to construct the fetal brain atlas based on SR reconstructed 3D fetal brains. We selected five normal brains from every two gestational week bins to generate population templates. The atlas generation pipeline is shown in Fig. 3. Among the five brains in each bin, we carried out pairwise registrations (Serag et al. 2012a) by selecting one of the brains as a target image, and the rest of the brains were registered to the target brain, by affine and deformable registration using Symmetric image Normalization (SyN) (Avants et al. 2008) in the ANTs toolbox (https://github.com/ANTsX/ANTs). This procedure was applied to each of the five brains and produced a group average for every brain. Averaging the five groups averaged images generated the initial template ($I_A{}^1$). The use of pairwise registrations eliminated bias in the atlas toward any of the original images. In the first iteration, the five brains were registered to the $I_A{}^1$ from their native space using affine and deformable registration, and averaged to obtain an averaged template ($I_A{}^2$). In the second iteration, all brains were transformed to $I_A{}^2$ from their native space with affine and deformable registration, and averaged to get an averaged template ($I_A{}^3$). The procedure was repeated 15 times until the template became stable (Supplementary Fig. 1).

Mapping the morphological fetal brain development

To quantify the morphological changes of the fetal brain parenchyma, we removed the cerebrospinal fluid (CSF) on the fetal brain atlas. The atlas images were first segmented by the Developing Brain Region Annotation with Expectation–Maximization (Draw-EM) tool (Makropoulos et al. 2014) and the segmentation results were then manually corrected by a trained research assistant in ROIEditor (https://www.mristudio.org/). Note we did not perform the segmentation on individual fetal brains because the segmentation accuracy of the individual brains based on Draw-EM was poor and extensive manual corrections would be needed which is subject to manual errors.

Based on the CSF-free fetal brain atlas, morphological changes between gestational stages were quantified by the transformation between adjacent gestational stages. For instance, transforming the template at 23–24 weeks to the template at 25–26 weeks to obtain the morphological change from 23.5 weeks to 25.5 weeks. The transformation was achieved by rigid registration followed by SyN-based deformable registration. For each pair of transformations, the deformation field was computed using the log-Jacobian matrix of the deformable transformation. The determinant of the log-Jacobian matrix was used to quantify the amount of morphological differences between adjacent gestational stages. In addition, the dynamic changes from 23 to 36 weeks of gestation can be captured continuously by interpolating the log-Jacobian matrices, and predicted brain atlas can be obtained at any given GA.

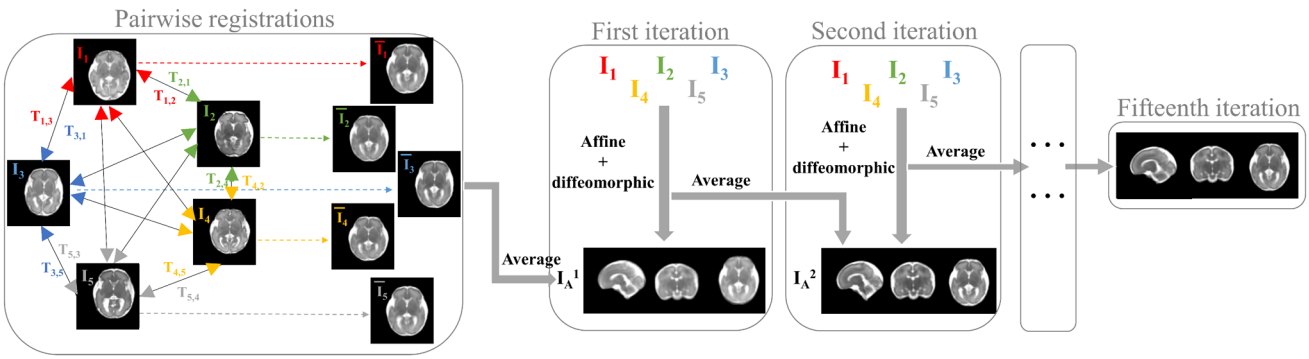

Fig. 3 Pipeline for fetal brain atlas generation. Five normal developing fetal brain images were chosen at a given gestational stage (every two weeks). Pairwise registrations using affine and deformable registration were performed to generate the initial template $I_A{}^1$. In the first iteration, the five fetal brains were registered to the $I_A{}^1$ from their native space by affine and deformable transformation to generate $I_A{}^2$. The procedure was iterated 15 times to produce the final template

Results

Figure 4 shows representative segmentation results of fetal brains at different GAs in the sagittal, coronal, and axial orientations. The automated segmentation by the U-net (magenta contours), mostly overlapped with the manually delineated ground truth (green contours). Table 1 demonstrates the segmentation performance of the U-net method compared with the NiftyMIC method in the test set, in three orientations. The U-net method yielded an average Dice score of 0.97 across the three brain orientations (0.9774, 0.9759, and 0.9564 in the coronal, sagittal, and axial orientations, respectively). In comparison, the average Dice score of NifityMIC based segmentation was 0.90 (0.9266, 0.9285, and 0.8330 in the coronal, sagittal, and axial orientations, respectively) and lower IOU, sensitivity, and specificity in all three orientations.

We observed a GA-dependent variation of the segmentation accuracy in our results (Fig. 5), especially in the axial images. The relatively low accuracy at early GA (before 25 weeks) was likely to be related to the relatively small number of training data (Fig. 1) and relatively large morphologic change at early GA compared to later stages. Besides, Dice scores in the coronal and sagittal orientations were higher than those in the axial orientation, which was possibly due to the difficulty in segmenting the bottom part of the fetal brain in the axial orientation, e.g., the medulla oblongata and the cerebellum. Nevertheless, the overall high segmentation accuracy was sufficient for SR reconstruction.

Based on the U-net masked images, we constructed the 3D fetal brain images using SR reconstruction

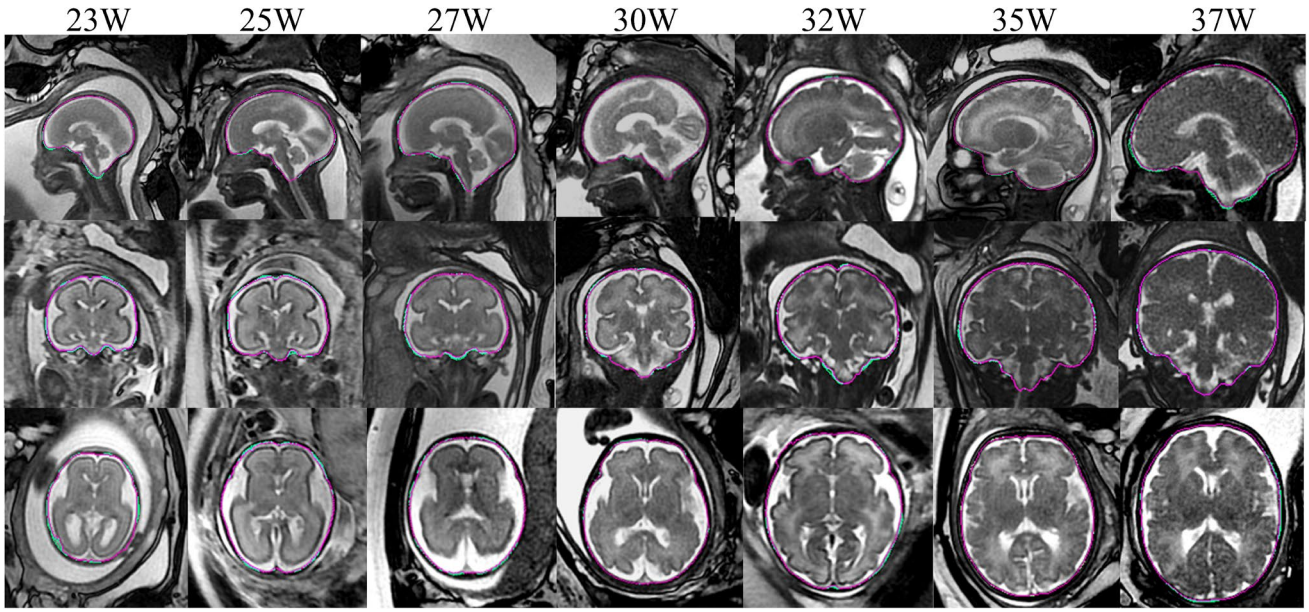

Fig. 4 The contours of the U-net predicted brain mask (in magenta) and the ground truth (in green) are shown for fetal brains at different gestational weeks, in sagittal, coronal, and axial orientations

Table 1 The performance of the U-net model and the NiftyMIC toolbox. The Dice score, IOU, specificity, and sensitivity of the segmentation results in three orientations were compared between the two methods

	Dice			IOU		
Methods	Coronal	Sagittal	Axial	Coronal	Sagittal	Axial
U-net	0.9774 ± 0.0074	0.9759 ± 0.0121	0.9564 ± 0.0176	0.9558 ± 0.0139	0.9531 ± 0.0226	0.9170 ± 0.0320
NiftyMIC	0.9266 ± 0.0633	0.9285 ± 0.0769	0.8330 ± 0.1468	0.8685 ± 0.0924	0.8742 ± 0.1090	0.7364 ± 0.1860
	Specificity			Sensitivity		
Methods	Coronal	Sagittal	Axial	Coronal	Sagittal	Axial
U-net	0.9994 ± 0.0003	0.9992 ± 0.0004	0.9982 ± 0.0009	0.9762 ± 0.0109	0.9744 ± 0.0216	0.9723 ± 0.0128
NiftyMIC	0.9976 ± 0.0042	0.9975 ± 0.0090	0.9882 ± 0.0154	0.9762 ± 0.0176	0.9150 ± 0.0393	0.9477 ± 0.0194

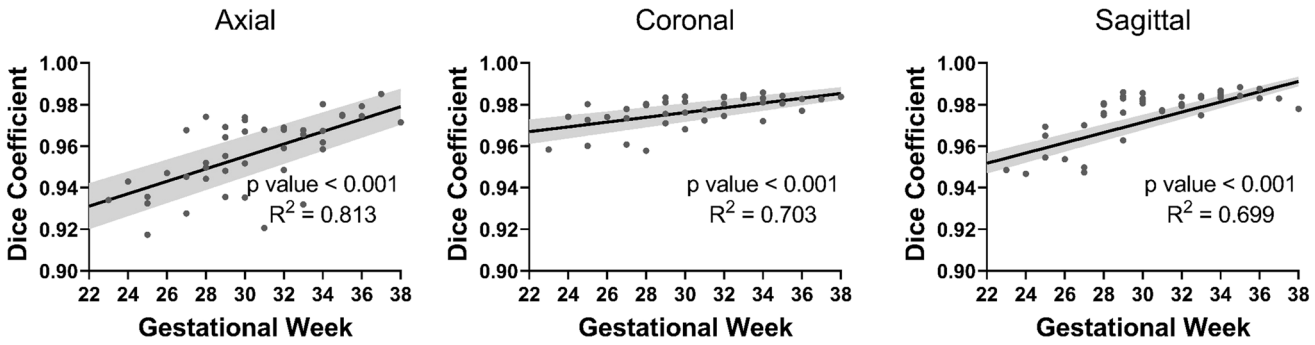

Fig. 5 Relation between the Dice scores from the U-net segmentation and GA in three orientations. The solid line indicates the mean and the shaded region indicates the standard deviation of the Dice scores at varying gestational weeks

(Supplementary Fig. 2). We then constructed the fetal brain atlas by computing the average brain templates every two weeks from 23 to 36 gestational weeks. The 4D spatiotemporal fetal brain atlas with an isotropic resolution of 0.8 mm is shown in Fig. 6, in sagittal, coronal, and axial views, which characterized the drastic changes in the shape and size of the fetal brains. It was observed that between 23 and 26 weeks of gestation, the development of calcarine fissure and cingulate gyrus were prominent; part of the primary sulci, precentral gyrus, and post-central gyrus were formed between 27 and 30 weeks of gestation; the rest of the primary sulci and part of the secondary sulci appeared between 31 and 34 weeks of gestation; and between 34 and 36 weeks of gestation, the ventricles gradually shrink due to the expansion of brain parenchyma. In addition, to fill the gestational gap (2 weeks) in the current atlas, we interpolated the transformation matrices between adjacent GA to generate pseudo-templates at a 0.5-week interval (Supplementary Fig. 3), or even finer intervals (Supplementary Video) for better visualization of the dynamic process.

The morphological changes between adjacent gestational stages are illustrated in Fig. 7 in 2D and 3D views. The color bar represents the amount of morphological deformation when transforming one template to the next, indicating the rate of brain growth from one gestational stage to the next. Dramatic fetal brain growth was observed during early gestation, e.g., from 23.5 to 27.5 weeks, and the growth rate slowed down towards late gestation. Moreover,

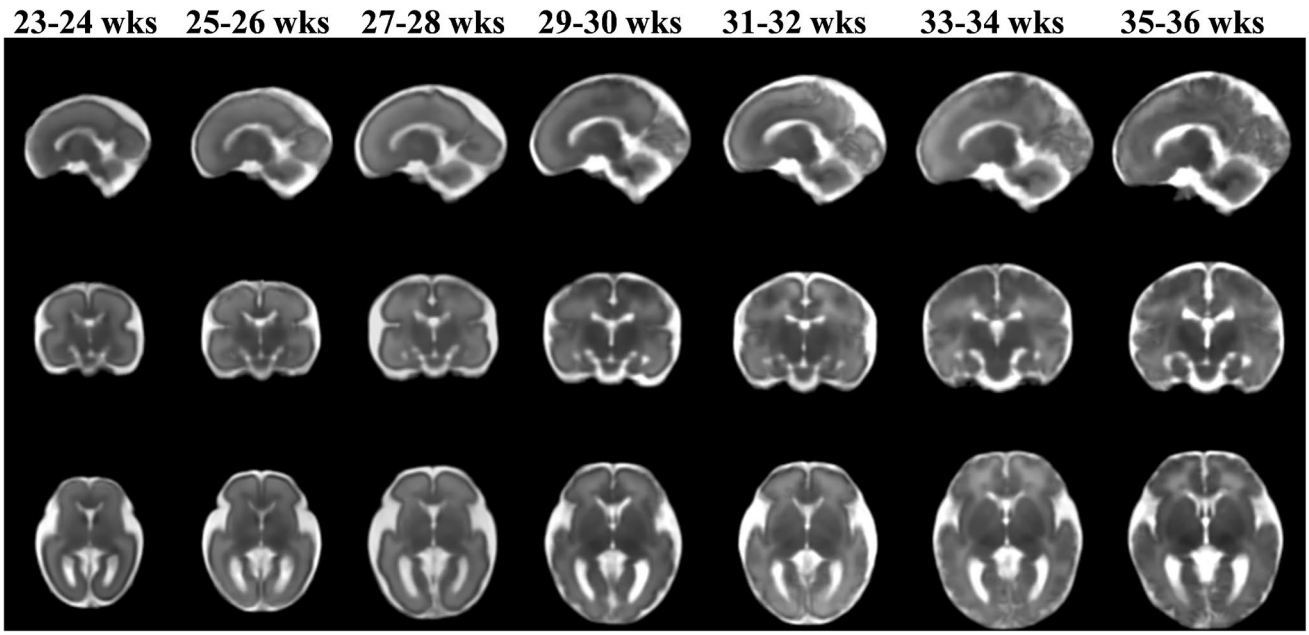

Fig. 6 Fetal brain atlas was generated for GAs of 23–24, 25–26, 27–28, 29–30, 31–32, 33–34, and 35–36 weeks, in sagittal, coronal, and axial views

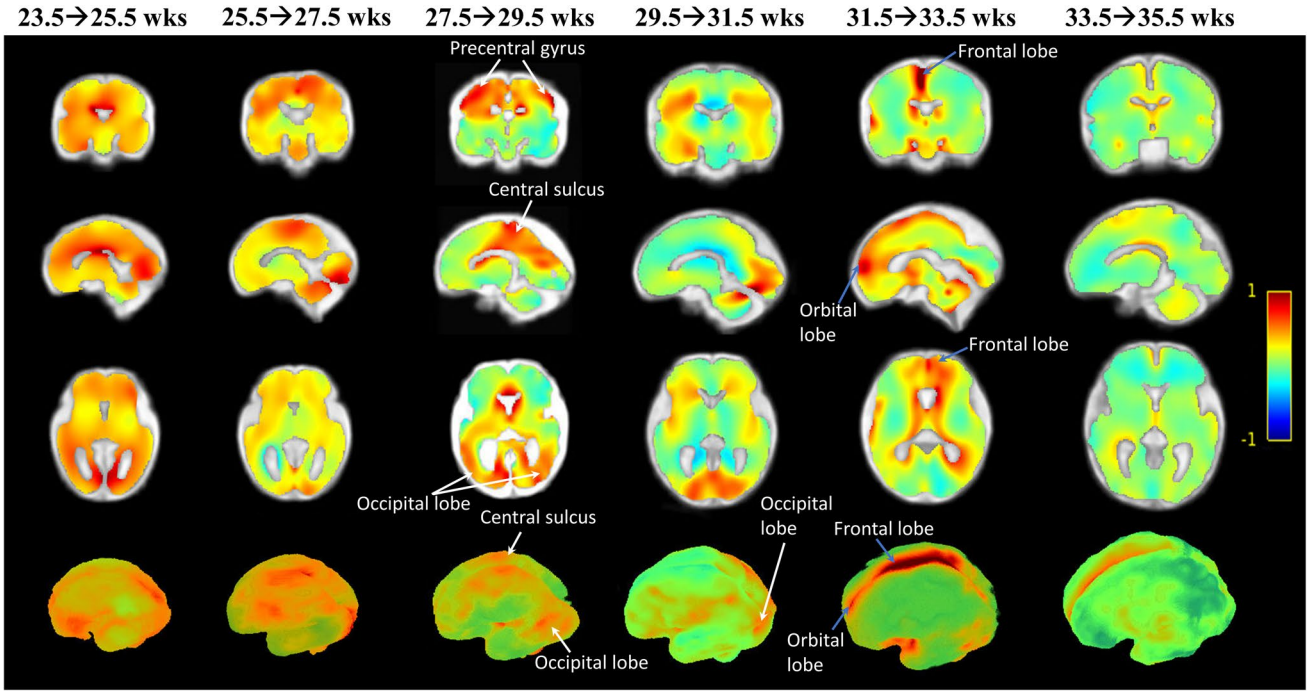

Fig. 7 The morphological changes of fetal brains between adjacent gestational stages. The determinant of the log-Jacobian matrix, which represented the amount of morphological change between adjacent fetal brain templates, was rendered in 2D and 3D views. The colors indicate the amount of morphological expansion (red) or retraction (blue, e.g., when cortical folding takes place)

a posterior-to-anterior developing pattern was observed. The log-Jacobian map of brain transformation from 27.5 to 29.5 weeks indicated the fastest changes in the central and posterior brain including the central sulcus, pre- and post-central gyri, and occipital lobe regions (white arrows), while the transformation from 31.5 to 33.5 weeks suggested prominent changes in the frontal-orbital regions (blue arrows).

Discussion

In this work, we proposed a fully automatic segmentation method based on U-net, and together with the SR reconstruction, 3D images of the fetal brains were obtained in an automated manner. Moreover, we generated a 4D spatiotemporal atlas in a Chinese population, based on which, we quantitatively mapped the fetal brain development from 23 to 36 weeks of gestation. To the best of our knowledge, the existing fetal brain atlases were collected from the Caucasian populations, which might not be entirely appropriate for analysis of fetal brain development in a different population, as indicated by many studies (Tang et al. 2010; Liang et al. 2015; Rao et al. 2017; Zhao et al. 2019b). Therefore, the establishment of a dedicated Chinese fetal brain atlas provided a normative brain template for the quantitative characterization of fetal brain development in related studies and comparison with abnormally developing fetuses as a tool for prenatal disease detection.

For quantitative assessment and the volumetric reconstruction of the fetal brain, accurate and automatic fetal brain segmentation is a prerequisite. Extracting the fetal brain from the in utero MRI image is an entirely different task than skull stripping in the adult brain. Due to the complex in utero compositions (amniotic fluid, placental, fetal body), the maternal body tissues surrounding the fetal brain, and the random fetal brain orientation, the fetal brain is often not the gravitational center of the image. Therefore, traditional brain extraction methods that rely on image registration (Wright et al. 2014; Taimouri et al. 2015; Tourbier et al. 2017) mostly fail. Deep-learning methods open a new avenue for this challenging task (Khalili et al. 2019; Zhao et al. 2019a; Salehi et al. 2017; Ebner et al. 2020). Salehi et al. segmented the fetal brain with two different Auto-Net architectures, including a voxelwise CNN architecture and a fully convolutional network based on the U-net architecture, which achieved Dice scores of 0.9597 and 0.9380, respectively, using a dataset of 75 images (Salehi et al. 2017). Ebner et al. proposed two separate CNNs for localization and segmentation of the fetal brain using 114 scans from normal and spina bifida fetuses for training and achieved a Dice coefficient around 0.935 (Ebner et al. 2020). Both studies have an optimized CNN structure, but the segmentation accuracies were moderate, possibly due to the limited

training data. There were also other studies using deep learning methods for fetal brain tissue segmentation (Khalili et al. 2019; Zhao et al. 2019a). Here, we proposed a U-net model to segment the fetal brain from 212 scans, which achieved an average Dice of 0.97 (±0.01) and robust performance for images in all three orientations across a full gestational age from 23 to 38 weeks. Considering that the segmentation was performed on routine clinical scans with relatively thick slices and variable image qualities, the segmentation accuracy was comparable or even superior to the existing method (Table 1) and was sufficient for the subsequent volumetric reconstruction. Besides, the 2D U-net was computationally efficient, which only took 2–3 s to extract one fetal brain. This accurate, robust, and convenient tool is readily translatable to clinical studies.

The generation of fetal brain atlases becomes feasible with the automated fetal brain extraction and volumetric reconstruction pipeline. We took a deformable registration approach to generate a 4D spatiotemporal fetal brain atlas from 23 to 36 weeks of gestation. A number of population brain atlas generation methods have been proposed (Schuh et al. 2018; Makropoulos et al. 2016; Gousias et al. 2012; Serag et al. 2012a). Especially, for the generation of the fetal brain atlases, Habas et al. developed age-specific MR templates and tissue probability maps of the fetal brain, based on group-wise registration of manual segmentations and voxel-wise nonlinear modeling (Habas et al. 2010). Gholipour et al. developed an algorithm to construct an unbiased four-dimensional atlas of the developing fetal brain by integrating symmetric diffeomorphic deformable registration in space with kernel regression in age (Gholipour et al. 2017). Here we used iterative deformable registration to ensure gradual convergence of the individual brains to the template. The fact that the iteration converged in 15 iterations indicated the average template became representative of the individual brains at a given GA. This approach has been used in generating neonatal brain atlases (Alexander et al. 2017) and the SyN algorithm has been demonstrated to be among the best performing deformable registration methods (Klein et al. 2009; Ou et al. 2014). For a 4D atlas with a temporal dimension, some strategies have been proposed to improve the temporal consistency of atlases between timepoints, such as the adaptive kernel regression method (Serag et al. 2012a) and the GroupWise approach (Schuh et al. 2018). However, since we had a limited number of brains ($n = 35$ across 23–36 weeks) and their GA information was limited to integers of weeks, these strategies did not apply to our dataset.

High-quality fetal brain atlases in the Caucasian or mixed population have been reported (Serag et al. 2012a, b; Gholipour et al. 2014, 2017; Khan et al. 2019). Several comparative studies showed considerable anatomical differences between races in children and adults, in terms of the bran size, shape, and topology (Tang et al. 2010; Liang et al. 2015; Rao et al. 2017; Zhao et al. 2019b). For instance, Zhao et al. showed that in pediatric brains between 6–12 years old, the major anatomical differences between Chinese and Caucasian brain templates were located in the bilateral frontal and parietal areas (Zhao et al. 2019b). Tang et al. found significant differences in brain shape and size between Chinese and Caucasian young males, such as the brain length, width, height, AC-PC line distance, and their perspective ratios (Tang et al. 2010). It is possible that the developmental differences begin in the fetal period, and, therefore, it is essential to build a racial specific fetal brain atlas for related studies. It would be ideal to perform a comparison between the Chinese atlas with the existing ones. However, since all of our imaging data were retrospectively collected from pure clinical scans at 1.5 T which typically had low resolution (thick slices), the current version of our atlas could not match the existing high-resolution atlas (Gholipour et al. 2017) for a fair comparison. Higher-resolution data acquired with matched protocols are required to elucidate any ethnic differences. On the other hand, the current atlas is still sufficient for capturing the overall brain development and could serve as suitable references for analyzing clinical fetal MRI data acquired at a similar resolution, e.g., for abnormality detection purpose.

In addition to visual examination of the fetal brain development from the 4D atlas, we quantitatively characterized the morphological changes between gestational stages based on the deformation maps. Atlas-based morphological comparison based on population atlas is commonly used for quantifying developing/group differences, e.g., to characterize neonatal brain development (Schuh et al. 2014; Breu et al. 2013) or to compare the fetal and neonatal brains. The deformation maps between the fetal atlases of neighboring GAs revealed that the calcarine fissure, the primary gyrus, pre- and post-central gyri, and secondary gyrus developed in sequential order, which agreed with previous findings of the spatiotemporal developmental pattern (Bendersky et al. 2006; Monteagudo and Timor-Tritsch 1997). The fast changes in the central sulcus and the precentral/postcentral gyri indicated early development of the preliminary motor and sensory areas, while the subsequent changes in the superior and frontal gyri may relate to the development of higher-order functions. The timeline captured by the deformation maps agreed well with the critical milestones of fetal brain development (Garel et al. 2001, 2003).

In addition to the aforementioned issues, there are several other limitations in the current study. First, it would be attractive to quantify the development of individual brain regions, which however, would require detailed segmentation of individual brains. Automated segmentation of the fetal brain is difficult, especially given the limited resolution, and requires extensive manual correction; and therefore,

analysis of individual brains was not performed in our study. Second, the number of normal developing fetal brain samples was relatively small in our study. Therefore, we were only able to generate a population template for every two gestational weeks, assuming relatively small anatomical changes within the two-week periods. Finer GA intervals should be used when more data become available.

Conclusion

In this work, we proposed an automated fetal brain analysis pipeline, including brain extraction, 3D volumetric reconstruction, atlas generation, and quantification of brain morphological development. Using this automated approach, we were able to reconstruct fetal brains across gestation and generate a 4D fetal brain atlas between 23 and 36 gestational weeks in a Chinese population. The spatiotemporal atlas allowed us to depict the normal fetal brain development process and provided a normative reference for fetal brain examinations in clinical practice.

Supplementary Information The online version contains supplementary material available at https://doi.org/10.1007/s00429-021-02303-x.

Authors contribution HL: processed MRI data and performed analyses. DW: was in charge of the study design and overall progress of the study. HL and DW: drafted the manuscript. GY, KL, and YZ: contributed to the collection of the MRI data. All authors contributed to the interpretation and review of the manuscript.

Funding This work was supported by the Ministry of Science and Technology of the People's Republic of China (2018YFE0114600), National Natural Science Foundation of China (61801424, 81971606, 61801421, and 81971605), and the Leading Innovation and Entrepreneurship Team of Zhejiang Province (202006140).

Availability of data and material The data (anonymized) in this study can be accessed with a data-sharing agreement.

Code availability The code used in this work is available from the authors upon request.

Declarations

Conflicts of interest The authors declare no competing financial interests.

References

Alexander B, Murray AL, Loh WY, Matthews LG, Adamson C, Beare R, Chen J, Kelly CE, Rees S, Warfield SK (2017) A new neonatal cortical and subcortical brain atlas: the Melbourne Children's Regional Infant Brain (M-CRIB) atlas. Neuroimage 147:841–851

Avants BB, Epstein CL, Grossman M, Gee JC (2008) Symmetric diffeomorphic image registration with cross-correlation: evaluating automated labeling of elderly and neurodegenerative brain. Med Image Anal 12(1):26–41

Bendersky M, Musolino PL, Rugilo C, Schuster G, Sica RE (2006) Normal anatomy of the developing fetal brain Ex vivo anatomical–magnetic resonance imaging correlation. J Neurol Sci 250(1–2):20–26

Breu M, Reisinger D, Wu D, Zhang Y, Fatemi A, Zhang J (2013) In vivo diffusion tensor imaging of the neonatal rat brain development. Neuropediatrics 44(S01):A11

Chartier AL, Bouvier MJ, McPherson DR, Stepenosky JE, Taysom DA, Marks RM (2019) The safety of maternal and fetal MRI at 3 T. Am J Roentgenol 213(5):1170–1173

Chee MW, Chen KH, Zheng H, Chan KP, Isaac V, Sim SK, Chuah LY, Schuchinsky M, Fischl B, Ng TP (2009) Cognitive function and brain structure correlations in healthy elderly East Asians. Neuroimage 46(1):257–269

Cox RW (1996) AFNI: software for analysis and visualization of functional magnetic resonance neuroimages. Comput Biomed Res 29(3):162–173

Ebner M, Chung KK, Prados F, Cardoso MJ, Chard DT, Vercauteren T, Ourselin S (2018a) Volumetric reconstruction from printed films: enabling 30 year longitudinal analysis in MR neuroimaging. NeuroImage 165:238–250

Ebner M, Wang G, Li W, Aertsen M, Patel PA, Aughwane R, Melbourne A, Doel T, David AL, Deprest J (2018b) An automated localization, segmentation and reconstruction framework for fetal brain MRI. International conference on medical image computing and computer-assisted intervention. Springer, pp 313–320

Ebner M, Wang G, Li W, Aertsen M, Patel PA, Aughwane R, Melbourne A, Doel T, Dymarkowski S, De Coppi P (2020) An automated framework for localization, segmentation and super-resolution reconstruction of fetal brain MRI. NeuroImage 206:116324

Fogliarini C, Chaumoitre K, Chapon F, Fernandez C, Lévrier O, Figarella-Branger D, Girard N (2005) Assessment of cortical maturation with prenatal MRI. Part I: Normal Cortical Matur 15(8):1671–1685

Garel C, Chantrel E, Brisse H, Elmaleh M, Luton D, Oury J-F, Sebag G, Hassan M (2001) Fetal cerebral cortex: normal gestational landmarks identified using prenatal MR imaging. Am J Neuroradiol 22(1):184–189

Garel C, Chantrel E, Elmaleh M, Brisse H, Sebag G (2003) Fetal MRI: normal gestational landmarks for cerebral biometry, gyration and myelination. Childs Nerv Syst 19(7–8):422–425

Gholipour A, Estroff JA, Warfield SK (2010) Robust super-resolution volume reconstruction from slice acquisitions: application to fetal brain MRI. IEEE Trans Med Imaging 29(10):1739–1758

Gholipour A, Limperopoulos C, Clancy S, Clouchoux C, Akhondi-Asl A, Estroff JA, Warfield SK (2014) Construction of a deformable spatiotemporal MRI atlas of the fetal brain: evaluation of similarity metrics and deformation models. International conference on medical image computing and computer-assisted intervention. Springer, pp 292–299

Gholipour A, Rollins CK, Velasco-Annis C, Ouaalam A, Akhondi-Asl A, Afacan O, Ortinau CM, Clancy S, Limperopoulos C, Yang E (2017) A normative spatiotemporal MRI atlas of the fetal brain for automatic segmentation and analysis of early brain growth. Sci Rep 7(1):476

Glenn OA (2006) Fetal central nervous system MR imaging. Neuroimaging Clinics 16(1):1–17

Gousias IS, Edwards AD, Rutherford MA, Counsell SJ, Hajnal JV, Rueckert D, Hammers A (2012) Magnetic resonance imaging of the newborn brain: manual segmentation of labelled atlases in term-born and preterm infants. Neuroimage 62(3):1499–1509

Griffiths PD, Bradburn M, Campbell MJ, Cooper CL, Graham R, Jarvis D, Kilby MD, Mason G, Mooney C, Robson SC (2017) Use of MRI in the diagnosis of fetal brain abnormalities in utero

(MERIDIAN): a multicentre, prospective cohort study. Lancet 389(10068):538–546
Habas PA, Kim K, Corbett-Detig JM, Rousseau F, Glenn OA, Barkovich AJ, Studholme C (2010) A spatiotemporal atlas of MR intensity, tissue probability and shape of the fetal brain with application to segmentation. Neuroimage 53(2):460–470
Iglesias JE, Liu C-Y, Thompson PM, Tu Z (2011) Robust brain extraction across datasets and comparison with publicly available methods. IEEE Trans Med Imaging 30(9):1617–1634
Jarvis DA, Griffiths PD (2019) Current state of MRI of the fetal brain in utero. J Magn Reson Imaging 49(3):632–646
Jenkinson M, Pechaud M, Smith S (2005) BET2: MR-based estimation of brain, skull and scalp surfaces. In: Eleventh annual meeting of the organization for human brain mapping, vol 17, pp 167
Jiang S, Xue H, Glover A, Rutherford M, Rueckert D, Hajnal JV (2007) MRI of moving subjects using multislice snapshot images with volume reconstruction (SVR): application to fetal, neonatal, and adult brain studies. IEEE Trans Med Imaging 26(7):967–980
Kainz B, Steinberger M, Wein W, Kuklisova-Murgasova M, Malamateniou C, Keraudren K, Torsney-Weir T, Rutherford M, Aljabar P, Hajnal JV (2015) Fast volume reconstruction from motion corrupted stacks of 2D slices. IEEE Trans Med Imaging 34(9):1901–1913
Khalili N, Lessmann N, Turk E, Claessens N, de Heus R, Kolk T, Viergever M, Benders M, Išgum I (2019) Automatic brain tissue segmentation in fetal MRI using convolutional neural networks. Mag Reson Imaging 64(77):89
Khan S, Vasung L, Marami B, Rollins CK, Afacan O, Ortinau CM, Yang E, Warfield SK, Gholipour A (2019) Fetal brain growth portrayed by a spatiotemporal diffusion tensor MRI atlas computed from in utero images. Neuroimage 185:593–608
Kleesiek J, Urban G, Hubert A, Schwarz D, Maier-Hein K, Bendszus M, Biller A (2016) Deep MRI brain extraction: a 3D convolutional neural network for skull stripping. Neuroimage 129:460–469
Klein A, Andersson J, Ardekani BA, Ashburner J, Avants B, Chiang M-C, Christensen GE, Collins DL, Gee J, Hellier P (2009) Evaluation of 14 nonlinear deformation algorithms applied to human brain MRI registration. Neuroimage 46(3):786–802
Kochunov P, Castro C, Davis D, Dudley D, Brewer J, Zhang Y, Kroenke CD, Purdy D, Fox PT, Simerly C (2010) Mapping primary gyrogenesis during fetal development in primate brains: high-resolution in utero structural MRI study of fetal brain development in pregnant baboons. Front Neurosci 4:20
Kuklisova-Murgasova M, Quaghebeur G, Rutherford MA, Hajnal JV, Schnabel JA (2012) Reconstruction of fetal brain MRI with intensity matching and complete outlier removal. Med Image Anal 16(8):1550–1564
Lee JS, Lee DS, Kim J, Kim YK, Kang E, Kang H, Kang KW, Lee JM, Kim J-J, Park H-J (2005) Development of Korean standard brain templates. J Korean Med Sci 20(3):483–488
Liang P, Shi L, Chen N, Luo Y, Wang X, Liu K, Mok VC, Chu WC, Wang D, Li K (2015) Construction of brain atlases based on a multi-center MRI dataset of 2020 Chinese adults. Sci Rep 5:18216
Lin G, Adiga U, Olson K, Guzowski JF, Barnes CA, Roysam B (2003) A hybrid 3D watershed algorithm incorporating gradient cues and object models for automatic segmentation of nuclei in confocal image stacks. Cytom Part A: J Int Soc Anal Cytol 56(1):23–36
Makropoulos A, Gousias IS, Ledig C, Aljabar P, Serag A, Hajnal JV, Edwards AD, Counsell SJ, Rueckert D (2014) Automatic whole brain MRI segmentation of the developing neonatal brain. IEEE Trans Med Imaging 33(9):1818–1831
Makropoulos A, Aljabar P, Wright R, Hüning B, Merchant N, Arichi T, Tusor N, Hajnal JV, Edwards AD, Counsell SJ (2016) Regional growth and atlasing of the developing human brain. Neuroimage 125:456–478
Makropoulos A, Counsell SJ, Rueckert D (2018) A review on automatic fetal and neonatal brain MRI segmentation. Neuroimage 170:231–248
Monteagudo A, Timor-Tritsch I (1997) Development of fetal gyri, sulci and fissures: a transvaginal sonographic study. Ultrasound Obstet Gynecol: off J Int Soc Ultrasound Obstet Gynecol 9(4):222–228
Nielsen BW, Scott RC (2017) Brain abnormalities in fetuses: in-utero MRI versus ultrasound. Lancet 389(10068):483–485
Ou Y, Akbari H, Bilello M, Da X, Davatzikos C (2014) Comparative evaluation of registration algorithms in different brain databases with varying difficulty: results and insights. IEEE Trans Med Imaging 33(10):2039–2065
Rao NP, Jeelani H, Achalia R, Achalia G, Jacob A, dawn Bharath R, Varambally S, Venkatasubramanian G, Yalavarthy PK (2017) Population differences in brain morphology: Need for population specific brain template. Psychiatr Res: Neuroimaging 265:1–8
Rolo LC, Araujo E, Nardozza LMM, de Oliveira PS, Ajzen SA, Moron AF (2011) Development of fetal brain sulci and gyri: assessment through two and three-dimensional ultrasound and magnetic resonance imaging. Arch Gynecol Obstet 283(2):149–158
Ronneberger O, Fischer P, Brox T (2015) U-net: Convolutional networks for biomedical image segmentation. International conference on medical image computing and computer-assisted intervention. Springer, pp 234–241
Rousseau F, Glenn OA, Iordanova B, Rodriguez-Carranza C, Vigneron DB, Barkovich JA, Studholme C (2006) Registration-based approach for reconstruction of high-resolution in utero fetal MR brain images. Acad Radiol 13(9):1072–1081
Rousseau F, Kim K, Studholme C, Koob M, Dietemann J-L (2010) On super-resolution for fetal brain MRI. International conference on medical image computing and computer-assisted intervention. Springer, pp 355–362
Rousseau F, Oubel E, Pontabry J, Schweitzer M, Studholme C, Koob M, Dietemann J-L (2013) BTK: An open-source toolkit for fetal brain MR image processing. Comput Methods Programs Biomed 109(1):65–73
Salehi SSM, Erdogmus D, Gholipour A (2017) Auto-context convolutional neural network (auto-net) for brain extraction in magnetic resonance imaging. IEEE Trans Med Imaging 36(11):2319–2330
Schuh A, Murgasova M, Makropoulos A, Ledig C, Counsell SJ, Hajnal JV, Aljabar P, Rueckert D (2014) Construction of a 4D brain atlas and growth model using diffeomorphic registration. International workshop on spatio-temporal image analysis for longitudinal and time-series image data. Springer, pp 27–37
Schuh A, Makropoulos A, Robinson EC, Cordero-Grande L, Hughes E, Hutter J, Price AN, Murgasova M, Teixeira RPA, Tusor N (2018) Unbiased construction of a temporally consistent morphological atlas of neonatal brain development. https://doi.org/10.1101/251512
Scott JA, Habas PA, Kim K, Rajagopalan V, Hamzelou KS, Corbett-Detig JM, Barkovich AJ, Glenn OA, Studholme C (2011) Growth trajectories of the human fetal brain tissues estimated from 3D reconstructed in utero MRI. Int J Dev Neurosci 29(5):529–536
Serag A, Aljabar P, Ball G, Counsell SJ, Boardman JP, Rutherford MA, Edwards AD, Hajnal JV, Rueckert D (2012a) Construction of a consistent high-definition spatio-temporal atlas of the developing brain using adaptive kernel regression. Neuroimage 59(3):2255–2265
Serag A, Kyriakopoulou V, Rutherford M, Edwards A, Hajnal J, Aljabar P, Counsell S, Boardman J, Rueckert D (2012b) A multichannel 4D probabilistic atlas of the developing brain: application to fetuses and neonates. Ann BMVA 2012(3):1–14
Taimouri V, Gholipour A, Velasco-Annis C, Estroff JA, Warfield SK (2015) A template-to-slice block matching approach for automatic localization of brain in fetal MRI. In: 2015 IEEE 12th

international symposium on biomedical imaging (ISBI). IEEE, pp 144–147

Tang Y, Hojatkashani C, Dinov ID, Sun B, Fan L, Lin X, Qi H, Hua X, Liu S, Toga AW (2010) The construction of a Chinese MRI brain atlas: a morphometric comparison study between Chinese and Caucasian cohorts. Neuroimage 51(1):33–41

Tourbier S, Velasco-Annis C, Taimouri V, Hagmann P, Meuli R, Warfield SK, Cuadra MB, Gholipour A (2017) Automated template-based brain localization and extraction for fetal brain MRI reconstruction. Neuroimage 155:460–472

Uchiyama HT, Seki A, Tanaka D, Koeda T (2013) A study of the standard brain in Japanese children: Morphological comparison with the MNI template. Brain Develop 35(3):228–235

Wang J, Perez L (2017) The effectiveness of data augmentation in image classification using deep learning. Convolutional Neural Network Vis Recognit 11

Weisstanner C, Kasprian G, Gruber G, Brugger P, Prayer D (2015) MRI of the fetal brain. Clin Neuroradiol 25(2):189–196

Wright R, Kyriakopoulou V, Ledig C, Rutherford MA, Hajnal JV, Rueckert D, Aljabar P (2014) Automatic quantification of normal cortical folding patterns from fetal brain MRI. Neuroimage 91:21–32

Wu D, Lei J, Rosenzweig JM, Burd I, Zhang J (2015) In utero localized diffusion MRI of the embryonic mouse brain microstructure and injury. J Mag Reson Imaging 42(3):717–728

Zhao L, Feng X, Meyer C, Wu Y, Plessis AJd, Limperopoulos C (2019a) Fetal brain automatic segmentation using 3D deep convolutional neural network. In: ISMRM 27th annual meeting, 2019, pp 11–16

Zhao T, Liao X, Fonov VS, Wang Q, Men W, Wang Y, Qin S, Tan S, Gao J-H, Evans A (2019b) Unbiased age-specific structural brain atlases for Chinese pediatric population. Neuroimage 189:55–70